



(1-C₅H₁₄N₂Br)₂MnBr₄: A Lead-Free Zero-Dimensional Organic-Metal Halide With Intense Green Photoluminescence

Xiaomei Jiang, Zhaolai Chen* and Xutang Tao*

State Key Laboratory of Crystal Materials & Institute of Crystal Materials, Shandong University, Jinan, China

OPEN ACCESS

Edited by:

Zhong Jin,
Nanjing University, China

Reviewed by:

Jianxu Ding,
Shandong University of Science and
Technology, China
Ju Dianxing,
Qingdao University of Science and
Technology, China
Theo Siegrist,
Florida State University, United States

*Correspondence:

Zhaolai Chen
zhaolaichen@sdu.edu.cn
Xutang Tao
txt@sdu.edu.cn

Specialty section:

This article was submitted to
Inorganic Chemistry,
a section of the journal
Frontiers in Chemistry

Received: 11 February 2020

Accepted: 03 April 2020

Published: 28 April 2020

Citation:

Jiang X, Chen Z and Tao X (2020)
(1-C₅H₁₄N₂Br)₂MnBr₄: A Lead-Free
Zero-Dimensional Organic-Metal
Halide With Intense
Green Photoluminescence.
Front. Chem. 8:352.
doi: 10.3389/fchem.2020.00352

Low-dimensional organic-inorganic hybrid materials have attracted tremendous attentions due to their fascinating properties as emerging star materials for light-emitting applications. Taking advantage of their rich chemical composition and structural diversity, here, a novel lead-free organic-manganese halide compound, (1-mPQBr)₂MnBr₄ (1-mPQ = 1-methylpiperazine, 1-C₅H₁₄N₂) with zero-dimensional structure has been rationally designed and successfully synthesized through solvent-evaporation method. Systematical characterizations were carried out to investigate the structure, thermal and photophysical properties. The (1-mPQBr)₂MnBr₄ was found to crystallized into an orthorhombic crystal (P₂₁2₁2₁) with lattice parameters of a = 8.272(6) Å, b = 15.982(10) Å and c = 17.489(11) Å. The structure consists of isolated [MnBr₄]²⁻ clusters and free Br⁻ ions as well as [C₅H₁₄N₂]²⁺ molecules. Thermal analysis indicates that it is stable up to 300°C. Upon ultraviolet photoexcitation, the (1-mPQBr)₂MnBr₄ exhibits intense green emission centered at 520 nm with a narrow full width at half-maximum of 43 nm at room temperature, which should be assigned to the spin-forbidden internal transition (⁴T₁(G) to ⁶A₁) of tetrahedrally coordinated Mn²⁺ ions. The superior photoluminescence properties coupled with facile and efficient synthesis method of this material suggest its considerable promise to be utilized as light-emitting materials.

Keywords: organic-metal halides, photoluminescence, single crystal, lead-free materials, manganese

INTRODUCTION

In recent decades, organic metal halide materials have flourished as star materials in solution-processed optoelectronics fields (Kojima et al., 2009; Chen et al., 2017; Yang et al., 2019a), arising from their superior properties including high absorption coefficient, long electron-hole diffusion length, ultralow trap density and high photoluminescence quantum yield (PLQY) as well as facile synthesis including low cost, high efficiency and flexibility (Dang et al., 2015; Liu et al., 2015, 2018; Huang et al., 2017). Benefitting from their remarkable advantages, they have shown great potential for photovoltaic solar cells (Kojima et al., 2009; Cheng et al., 2019; Yang et al., 2019b), light-emitting diodes (Ling et al., 2016; Thirumal et al., 2017; Lin et al., 2018), photodetectors (Adinolfi et al., 2016; Ahmadi et al., 2017; Shrestha et al., 2017), field-effect transistors (Yu et al., 2018; Zhu et al., 2019), and lasers (Yakunin et al., 2015; Zhu et al., 2015; Gu et al., 2016). Lately, the certified power

conversion efficiency of organic lead halide solar cells have achieved 25.2%¹, which outperforms that of CdTe and CuInGaSe₂ solar cells. In spite of their rapid development, the presence of toxic lead in these materials is deemed to be a serious concern, becoming a huge hindrance in their way to wide-scale exploitation. Based on this circumstance, it is therefore of urgent need to look for the alternative lead-free hybrids for future commercial optoelectronic applications.

Hence, immense efforts in reducing lead contents or exploring lead-free substitutes offer a viable solution for high-performance eco-friendly optoelectronic devices. Noteworthy, this class of materials endows with rich chemical and structural diversities. In addition to modifying the length of the organic components, the diverse structural dimensionality, referring to three-dimensional (3D), two-dimensional (2D), one-dimensional (1D) and zero-dimensional (0D) structures, can also be achieved by tuning the inorganic frameworks, which results in fascinating properties. In the first place, the most obvious alternative substitution to Pb²⁺, should be the elements in the same group in the periodic table, namely Sn²⁺ and Ge²⁺ (Zhumekenov et al., 2017; Fu et al., 2018; Ju et al., 2018a; Nazarenko et al., 2019). In addition, heterovalent elements in Group 15 (Bi³⁺ and Sb³⁺) (Abulikemu et al., 2016; Sun et al., 2016; Ji et al., 2017, 2018; Ju et al., 2018b; Zhang et al., 2018; Tao et al., 2019) and in Group 13 (In³⁺) (Zhou et al., 2019) have also been demonstrated as the alternative metals. Moreover, a range of divalent transition metal ions [Cu²⁺ (Cortecchia et al., 2016; Jun et al., 2018; Li et al., 2018; Park et al., 2018), Fe²⁺ (Han et al., 2014, 2015; Nakayama et al., 2017), Mn²⁺ (Bai et al., 2018; Park et al., 2018)] can also serve as substitutes for Pb²⁺. Among which, large number of researches have reported that organic manganese (Mn²⁺) halides possess brilliant photoluminescence ranging from green to red due to the variable metal-ion coordination geometry, with the photoluminescence lifetimes varying from microseconds to milliseconds. Many groups have made great efforts in exploring octahedral-coordinated Mn (Han et al., 2015; Lv et al., 2016; Nakayama et al., 2017; Bai et al., 2018) single crystals, such as 3D-structured (CH₃)₃NCH₂ClMnCl₃ (You et al., 2017) and (3-Pyrrolinium)MnX₃ (X = Cl, Br) (Ye et al., 2015), 2D-structured NH₃(CH₂)₅NH₃MnCl₄ (You et al., 2017) and (C₆H₅CH₂CH₂NH₃)₂MnCl₄ (Lv et al., 2016), 1D-structured (N-Methylpyrrolidinium)MnCl₃ (Ye et al., 2015), and (pyrrolidinium)MnBr₃ (Sun et al., 2017), as well as 0D-structured (C₄NOH₁₀)₅Mn₂Cl₉·C₂H₅OH (Zhang et al., 2015), etc. In comparison, less attention has been paid on the search and investigation of tetraordinated Mn²⁺ counterparts (Xu et al., 2017; Gong et al., 2019; Jana et al., 2019; Sun et al., 2019).

It is well-known that single crystals can exhibit better intrinsic properties of materials compared with the polycrystalline counterparts. Hence, in this work, we first rationally designed and synthesized a novel organic manganese halide, (1-mPQBr)₂MnBr₄ (1-mPQ=1-methylpiperazine, 1-C5H14N2) single crystal with a 0D structure. Systematical characterizations were applied to investigate the structures, photophysical and

thermal properties. The facile solvent-evaporation method, the intense green emission with high PLQY of 60.70% as well as good stability makes the (1-mPQBr)₂MnBr₄ suitable as green phosphors.

MATERIALS AND METHODS

Materials

Analytical-grade manganese (II) monoxide (MnO, 99.0%, Sinopharm Co. Ltd.), 1-methylpiperazine (1-C5H12N2, 99.0%, Sinopharm Co. Ltd.), hydrobromic acid (HBr, 40 wt% in H₂O, Sinopharm Co. Ltd.), and hypophosphorous acid aqueous solution (H₃PO₂, 50% in H₂O, Sinopharm Co. Ltd.) were used as received without any further processing or refining.

Preparation of (1-mPQBr)₂MnBr₄ Single Crystal

As a typical process, the yellow crystals of (1-mPQBr)₂MnBr₄ were obtained by slowly evaporating HBr/H₃PO₂ (3:1) mixed solutions containing 1-methylpiperazine and MnO with molar amounts of 2:1.

Characterizations

Powder X-ray diffraction (PXRD) patterns were performed on a Bruker-AXS D8 Advance X-ray diffractometer with CuKα1 radiation (λ = 1.54186 Å) in the range of 10–90° (2θ).

Single crystal's structure was determined by Bruker SMART APEX-II diffractometer equipped with a CCD detector (graphite-monochromatized Mo-Kα radiation, λ = 0.71073 Å) at 300 K. Data integration and cell refinement were performed using the APEX₂ software. The structure was analyzed by direct methods and refined using the SHELXTL 97 software package. All non-hydrogen atoms of the structure were refined with anisotropic thermal parameters, and the refinements converged for Fo² > 2σ_IFo². All the calculations were performed using SHELXTL crystallographic software package. Symmetry analysis on the model using PLATON revealed that no obvious space group change was needed. The crystallographic data was deposited in Cambridge Crystallographic Data Center (CCDC #1979443).

Fourier transform infrared (FTIR) spectrum in the region 700–4,000 cm⁻¹ was examined on a spectrometer (Nicolet 330) with KBr pellets.

X-ray photoelectron spectroscopy (XPS) measurements of the newly synthesized (1-mPQBr)₂MnBr₄ samples about 2 × 1 × 1 mm³ in size were performed on an ESCALAB 250 (Thermo Fisher Scientific) instrument under vacuum (1.7 × 10⁻¹⁰ mbar).

UV-vis diffuse reflectance spectroscopy was recorded using a Shimadzu UV 2550 spectrophotometer equipped with an integrating sphere over the spectral range 200–800 nm. The (1-mPQBr)₂MnBr₄ single crystals were ground into powders for tests. A BaSO₄ plate was used as the standard (100% reflectance). The absorption spectrum was calculated from the reflectance spectrum by using the Kubelka-Munk function: α/S = (1-R)²/(2R), where α is the absorption coefficient, S is the scattering coefficient, and R is the reflectance.

¹National Renewable Energy Labs (NREL) Efficiency Chart. Available online at: <https://www.nrel.gov/pv/assets/pdfs/best-research-cell-efficiencies.20200203.pdf>.

Photoluminescence Measurements

The excitation wavelength dependent-photoluminescence (PL) spectra and PL excitation spectra (PLE) were carried out by a laser of 365 nm with a photomultiplier (PMT-H-S1-CR131) and DSP lock-in amplifier (SRS 830). The time-resolved photoluminescence measurements (TRPL) were carried by FLS920 all functional fluorescence spectrometer (Edinburgh). The output laser wavelength was set to be 520 nm. The photoluminescence quantum yields (PLQY) were tested by an absolute PLQY measurement system (FLSP920) in an integrating sphere.

Thermalgravimetric Analysis (TGA) and Differential Scanning Calorimetry (DSC) Measurements

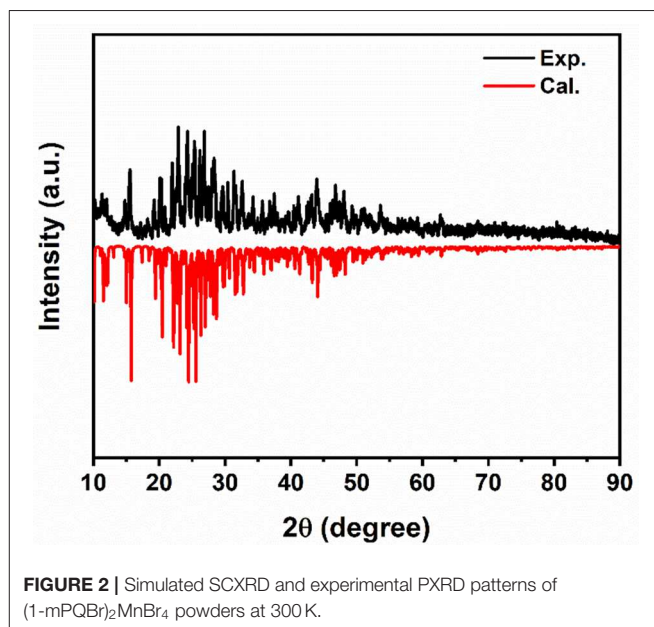
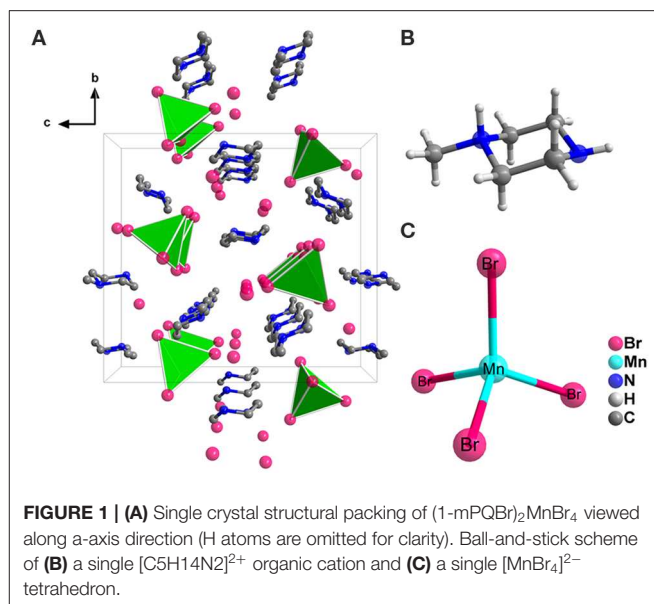
TGA and DSC curves were collected using a TGA/DSC1/1600HT analyzer (Mettler Toledo Instruments). The polycrystalline sample was placed in an aluminum crucible and heated at a rate of 10 K/min from room temperature to 800°C under flowing nitrogen gas.

RESULTS AND DISCUSSION

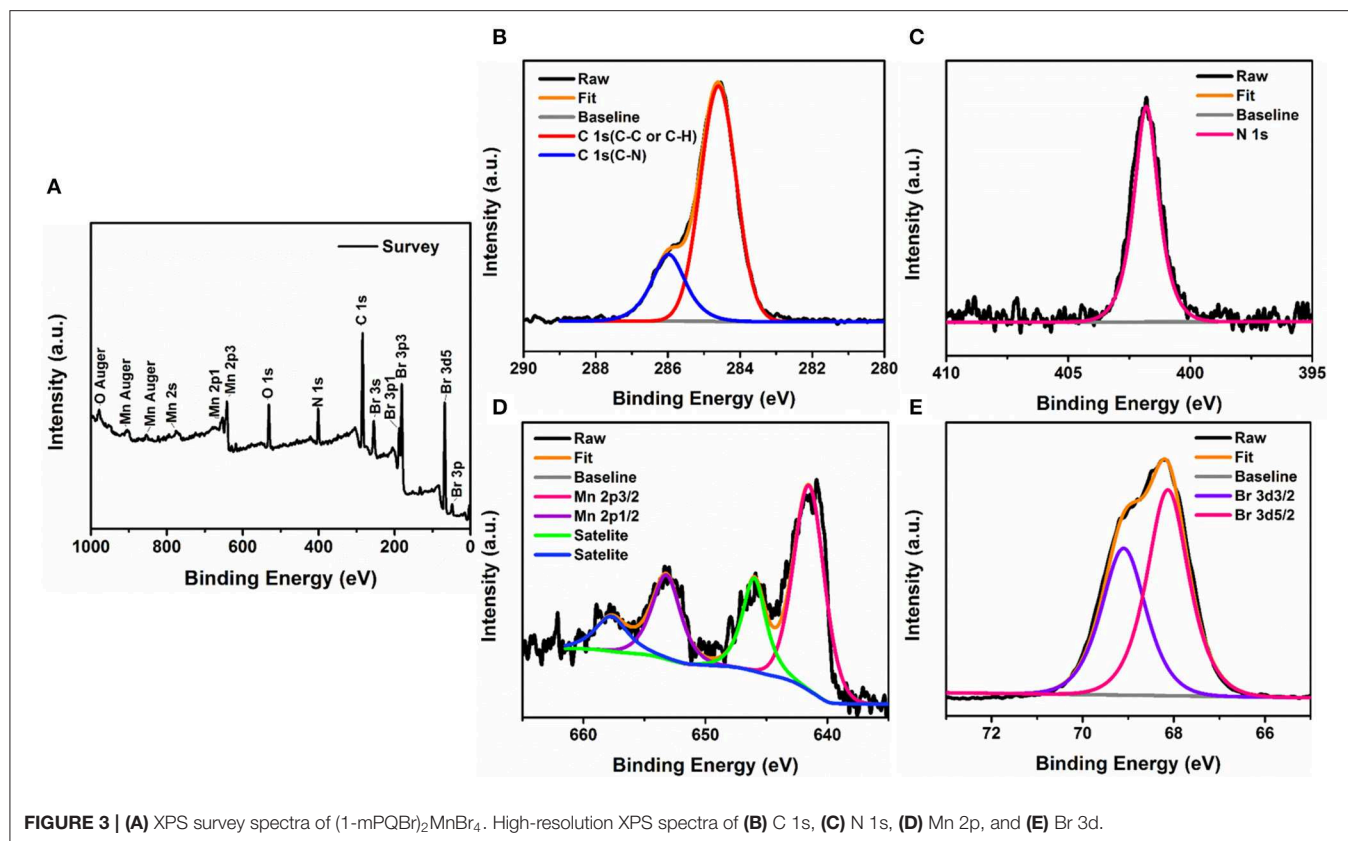
Crystal structure of the (1-mPQBr)₂MnBr₄ single crystal was obtained through SCXRD test, which belongs to the orthorhombic crystal system (a non-polar D₂ and chiral space group P2₁2₁2₁) at room temperature, with lattice parameters of a = 8.272(6) Å, b = 15.982(10) Å and c = 17.489(11) Å. In this structure, four formula units of (1-mPQBr)₂MnBr₄ are present in the unit cell. Further details for crystallographic parameters are provided in **Tables S1–S3** (in the Supporting Information) and the crystal structure and local structure descriptions are displayed in **Figure 1**. It is clearly seen that each Mn atom is coordinated by four Br atoms to form an isolated [MnBr₄]²⁻ tetrahedral cluster as inorganic part of the title compound. Such isolated [MnBr₄]²⁻ tetrahedral are surrounded by free Br⁻ and [C₅H₁₄N₂]²⁺ molecules (organic part), featuring a 0D structure. In **Figure 2** shows that the experimental PXRD pattern corresponds well to that calculated from SCXRD result with slightly varying intensities.

The FTIR spectrum in **Figure S1** further verifies the existence of the organic component. The broad peak around 3,353 cm⁻¹ belongs to the N-H stretching peak. The peaks in the range of 2,950–2,820 cm⁻¹ are assigned to the CH₂ and CH₃ symmetric and asymmetric stretching vibrations and the peak around 1,410 cm⁻¹ is ascribed to CH bending vibrations. Also, the strong signal at nearly 1,630 cm⁻¹ indicates asymmetric NH₃⁺ deformation. **Figure S2** shows the scanning electron microscope photograph of (1-mPQBr)₂MnBr₄ crystal. **Table S4** provides the detailed results of energy dispersive X-ray spectroscopy to further confirm the composition of inorganic and organic parts, respectively.

Additionally, the XPS spectrum in **Figure 3A** evidences the signatures of carbon (C 1s), oxygen (O 1s), nitrogen (N 1s), manganese (Mn 2p), and bromide (Br 3d), and the appearance of adventitious oxygen in the spectrum is generally ascribed to



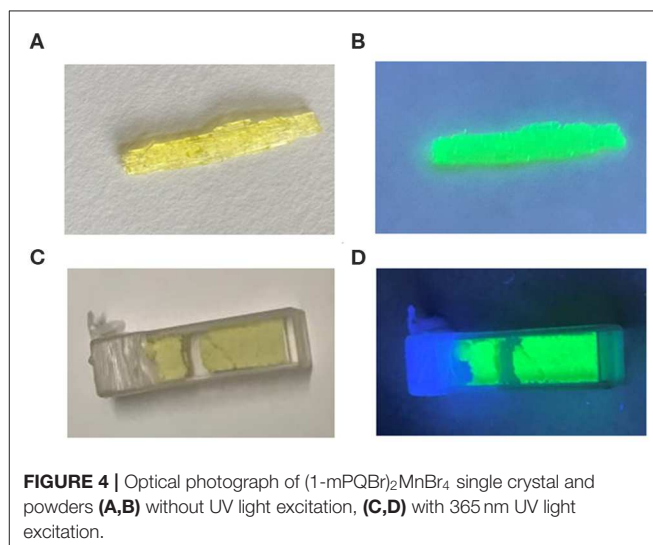
a contamination of the sample by physical adsorption during ambient exposure. We further recorded high-resolution spectra of the constituents in designated energy ranges (**Figures 3B–E**). The Mn doublet shows a spin-orbit splitting of 11.7 eV with the peaks corresponding to the binding energies of Mn 2p_{1/2} and 2p_{3/2} orbitals located at 653.3 and 641.6 eV, respectively. Similarly, the core-level spectrum of Br 3d contains a couple of split peaks at 69.2 and 68.1 eV corresponding to Br 3d_{3/2} and Br 3d_{5/2} orbitals with a separation of 1.1 eV, which are in good agreement with Br. By calculating the integrated peak areas of the XPS spectra, we can roughly estimate that Mn to Br possessed a molar ratio of 1:5.88. According to the analytical results of SCXRD, PXRD, EDS, and XPS, we can verify that



pure (1-mPQBr)₂MnBr₄ were successfully synthesized through the solvent-evaporation method.

Figure 4 displays the optical image of a rod-shaped (1-mPQBr)₂MnBr₄ single crystal and powders under ultraviolet light irradiation, and it is clearly seen that the title compound emits strong green light. To characterize the photophysical properties of (1-mPQBr)₂MnBr₄, the UV-vis absorption spectroscopy and PL spectroscopy were carried out at room temperature. In **Figure 5**, typical absorption spectra for organic manganese halides materials can be observed. The peaks below 340 nm originates from the transitions within the [C₅H₁₄N₂]²⁺ cation and peaks from 345 to 600 nm should be ascribed to the electronic transitions between the ground and the first excited triplet states of the Mn²⁺ ion in the crystal field, which is consistent with previous reports as listed in **Table S5**.

To further investigate the origin of this green emission, **Figures 6A,B** display the wavelength dependent PL spectra and PLE spectrum of (1-mPQBr)₂MnBr₄ single crystals. Upon excitation, the (1-mPQBr)₂MnBr₄ exhibits an intense green emission located at 520 nm with a narrow full width at half-maximum (FWHM) of 43 nm, corresponding to a characteristic transition from the ground state of the d-electron configuration (e_g)² (t_{2g})³ to the upper state of the configuration (e_g)³ (t_{2g})² (Wrighton and Ginley, 1974; Jiang et al., 2019). It is clearly noted that the PLE spectra are consistent with the absorption spectra. In the region between 300 and 500 nm, the discernable peaks correspond to radiative transitions from the ground state ⁶A₁



of tetrahedral Mn (II) to the excited states of ⁴T₁(G), ⁴T₂(4G), ⁴A₁(G), ⁴E(G), 4E(D), ⁴T₁(P), ⁴T₁(F), and ⁴A₂(F), respectively, according to the excited states of Mn²⁺ system (d⁵) in the Tanabe-Sugano diagram (Rodríguez-Lazcano et al., 2009).

The PLQY at room temperature is calculated to be about 60.70% and the Commission Internationale de l'Eclairage (CIE)

chromaticity coordinate for this green emission is determined to be (0.175, 0.589) (Figure 6C). Upon the excitation of 453 nm, the room-temperature TRPL decay curve is monitored for the

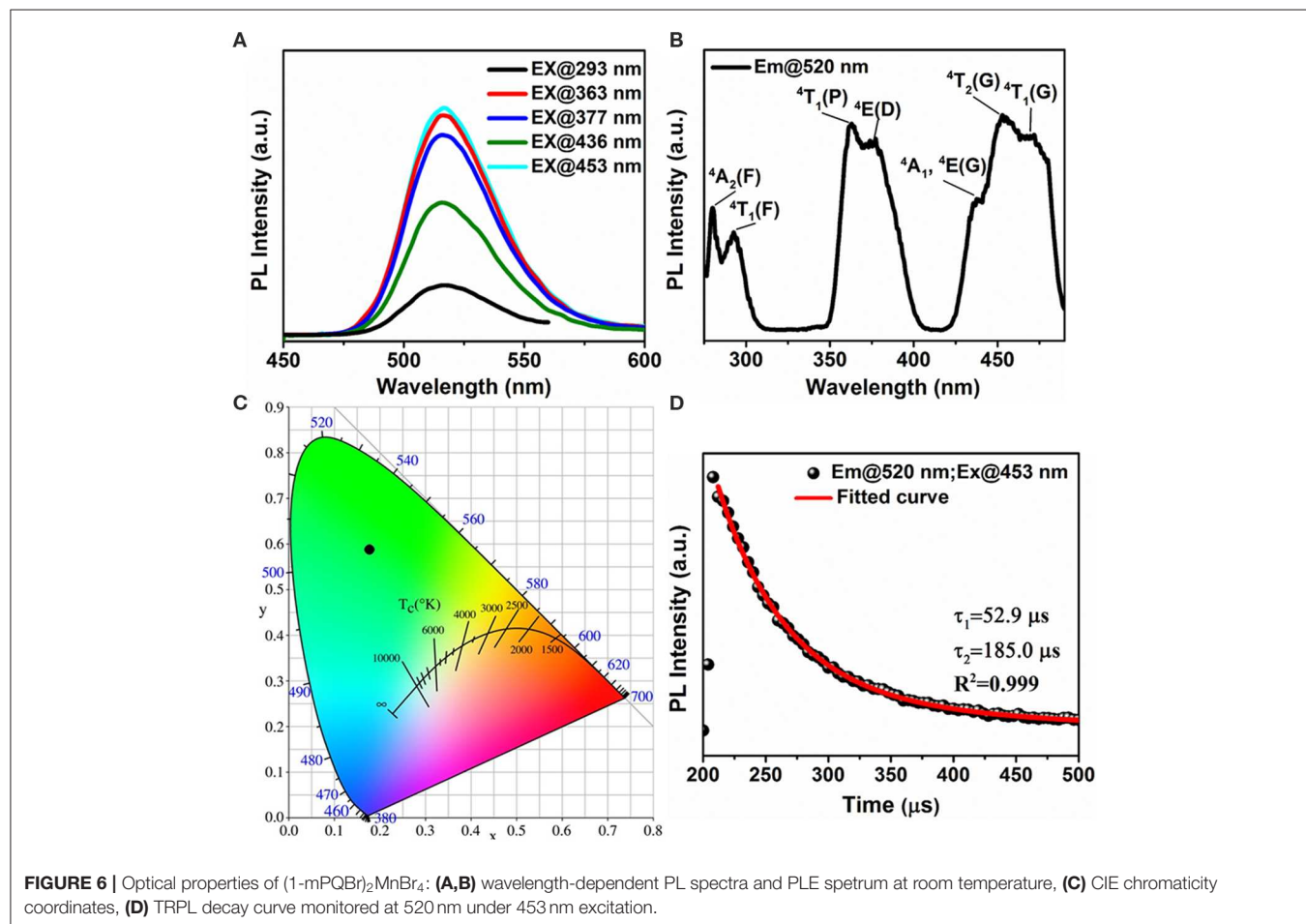
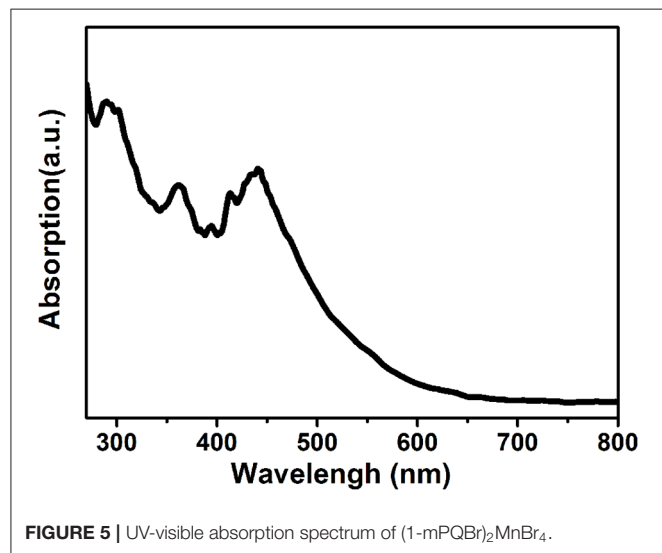
emission peak at 520 nm as shown in Figure 6D. The decay curve is modeled with the biexponential decay function:

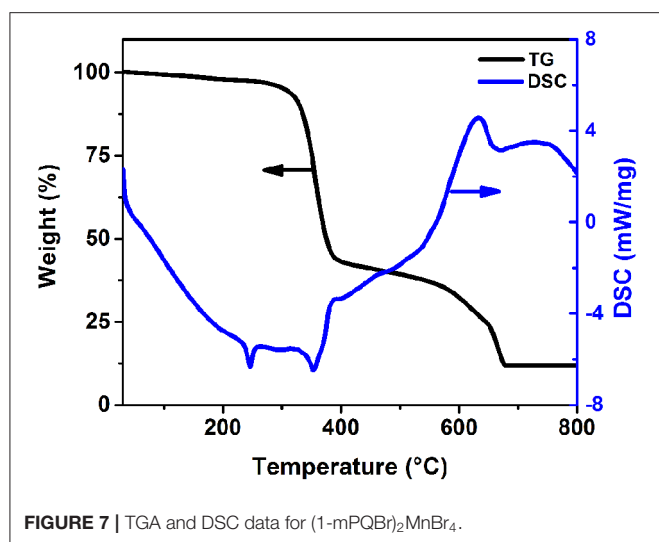
$$I(t) = A_1 e^{-\frac{t}{\tau_1}} + A_2 e^{-\frac{t}{\tau_2}}$$

where $I(t)$ is the time-resolved PL intensity, t is the time after excitation, A_1 and A_2 are the relative amplitudes, and τ_1 and τ_2 are lifetimes for fast and slow decays. The effective decay times are calculated to be 52.9 and 185.0 μ s, respectively.

Furthermore, such highly emissive bulk crystals and powders were examined to exhibit considerable thermal stability. TGA curve suggests that (1-mPQBr)₂MnBr₄ does not lose any mass until 300°C (Figure 7), which is comparatively higher than that of other organic-manganese halides reported in literature. This is hypothesized to be due to the large amounts of hydrogen bonding interaction between the organic and inorganic components in the 0D structure benefiting from the extra presence of free bromide ions. It possesses a two-step decomposition including the evaporation of organic parts and MnBr₂, respectively. In DSC scan, a sharp endothermic peak, which occurred at 250°C, corresponds to the melting point of (1-mPQBr)₂MnBr₄.

More importantly, the stability of hybrid metal halides is deemed as an important criterion for evaluation of their





potential for practical applications. Therefore, we evaluated the thermal stability of (1-mPQBr)₂MnBr₄ single crystals by annealing them at 150°C for 12 h on a hotplate. Notably, negligible change can be observed in the PXRD pattern (Figure S3). Moreover, after exposure to ambient conditions for 2 months, it still remain 96.3% of the original PL intensity (Figure S4).

CONCLUSIONS

In summary, we have synthesized a novel lead-free organic-manganese halide compound (1-mPQBr)₂MnBr₄ (1-mPQ=1-methylpiperazine, 1-C5H14N2), with 0D structure through solvent-evaporation method. A highly luminescent

green emission at 520 nm was observed for this novel organic-inorganic hybrid material, which should be resulted from the spin-forbidden internal transition (⁴T₁(G) to ⁶A₁) of tetrahedrally coordinated Mn²⁺ ions. We believe the superior photophysical properties and high stability makes it potential for light-emitting applications.

DATA AVAILABILITY STATEMENT

The datasets presented in this study can be found in online repositories. The name of the repository and accession number can be found below: Cambridge Crystallographic Data Centre (CCDC #1979443).

AUTHOR CONTRIBUTIONS

ZC and XT devised the project and proof outline. XJ synthesized the single crystals and conducted all the characterizations. All authors contributed to manuscript revision, read, and approved the submitted version.

FUNDING

This work was financially supported by the National Natural Science Foundation of China (Grant Nos. 51321091, 51772170, and 51272129), and Natural Science Foundation of Jiangsu Province (BK20190206).

SUPPLEMENTARY MATERIAL

The Supplementary Material for this article can be found online at: <https://www.frontiersin.org/articles/10.3389/fchem.2020.00352/full#supplementary-material>

REFERENCES

- Abulikemu, M., Ould-Chikh, S., Miao, X., Alarousu, E., Murali, B., Ngongang Ndjawa, G. O., et al. (2016). Optoelectronic and photovoltaic properties of the air-stable organohalide semiconductor (CH₃NH₃)₃Bi₂I₉. *J. Mater. Chem. A*, 4, 12504–12515. doi: 10.1039/C6TA04657F
- Adinolfi, V., Ouellette, O., Saidaminov, M. I., Walters, G., Abdelhady, A. L., Bakr, O. M., et al. (2016). Fast and sensitive solution-processed visible-blind perovskite UV photodetectors. *Adv. Mater.* 28, 7264–7268. doi: 10.1002/adma.201601196
- Ahmadi, M., Wu, T., and Hu, B. (2017). A review on organic-inorganic halide perovskite photodetectors: device engineering and fundamental physics. *Adv. Mater.* 29:1605242. doi: 10.1002/adma.201605242
- Bai, X. W., Zhong, H. Z., Chen, B. K., Chen, C., Han, J. B., Zeng, R. S., et al. (2018). Pyridine-modulated mn ion emission properties of C₁₀H₁₂N₂MnBr₄ and C₅H₆NMnBr₃ Single crystals. *J. Phys. Chem. C*, 122, 3130–3137. doi: 10.1021/acs.jpcc.7b11693
- Chen, Z., Dong, Q., Liu, Y., Bao, C., Fang, Y., Lin, Y., et al. (2017). Thin single crystal perovskite solar cells to harvest below-bandgap light absorption. *Nat. Commun.* 8:1890. doi: 10.1038/s41467-017-02039-5
- Cheng, X., Yang, S., Cao, B., Tao, X., and Chen, Z. (2019). Single crystal perovskite solar cells: development and perspectives. *Adv. Func. Mater.* 30:1905021. doi: 10.1002/adfm.201905021
- Cortecchia, D., Dewi, H. A., Yin, J., Bruno, A., Chen, S., Baikie, T., et al. (2016). Lead-Free MA₂CuCl_(x)Br_(4-x) hybrid perovskites. *Inorg. Chem.* 55, 1044–1052. doi: 10.1021/acs.inorgchem.5b01896
- Dang, Y., Liu, Y., Sun, Y., Yuan, D., Liu, X., Lu, W., et al. (2015). Bulk crystal growth of hybrid perovskite material CH₃NH₃PbI₃. *CrystEngComm*, 17, 665–670. doi: 10.1039/C4CE02106A
- Fu, P., Huang, M., Shang, Y., Yu, N., Zhou, H. L., Zhang, Y. B., et al. (2018). Organic-inorganic layered and hollow tin bromide perovskite with tunable broadband emission. *ACS Appl. Mater. Interfaces* 10, 34363–34369. doi: 10.1021/acsami.8b07673
- Gong, L. K., Hu, Q. Q., Huang, F. Q., Zhang, Z. Z., Shen, N. N., Hu, B., et al. (2019). Efficient modulation of photoluminescence by hydrogen bonding interactions between inorganic [MnBr₄]²⁻ anions and organic cations. *Chem. Commun.* 55, 7303–7306. doi: 10.1039/C9CC03038G
- Gu, Z., Wang, K., Sun, W., Li, J., Liu, S., Song, Q., et al. (2016). Two-Photon Pumped CH₃NH₃PbBr₃Perovskite microwire lasers. *Adv. Opt. Mater.* 4, 472–479. doi: 10.1002/adom.201500597
- Han, J., Nishihara, S., Inoue, K., and Kurmoo, M. (2014). On the nature of the structural and magnetic phase transitions in the layered perovskite-like (CH₃NH₃)₂[Fe(II)Cl₄]. *Inorg. Chem.* 53, 2068–2075. doi: 10.1021/ic402535u
- Han, J., Nishihara, S., Inoue, K., and Kurmoo, M. (2015). High magnetic hardness for the canted antiferromagnetic, ferroelectric, and ferroelastic

- layered perovskite-like (C₂H₅NH₃)₂[Fe(II)Cl₄]. *Inorg. Chem.* 54, 2866–2874. doi: 10.1021/ic5030229
- Huang, J., Yuan, Y., Shao, Y., and Yan, Y. (2017). Understanding the physical properties of hybrid perovskites for photovoltaic applications. *Nat. Rev. Mater.* 2:17042. doi: 10.1038/natrevmats.2017.42
- Jana, A., Zhumagali, S., Ba, Q., Nissimagoudar, A. S., and Kim, K. S. (2019). Direct emission from quartet excited states triggered by upconversion phenomena in solid-phase synthesized fluorescent lead-free organic-inorganic hybrid compounds. *J. Mater. Chem. A* 7, 26504–26512. doi: 10.1039/C9TA08268A
- Ji, C., Sun, Z., Zeb, A., Liu, S., Zhang, J., Hong, M., et al. (2017). Bandgap narrowing of lead-free perovskite-type hybrids for visible-light-absorbing ferroelectric semiconductors. *J. Phys. Chem. Lett.* 8, 2012–2018. doi: 10.1021/acs.jpcclett.7b00673
- Ji, C., Wang, P., Wu, Z., Sun, Z., Li, L., Zhang, J., et al. (2018). Inch-size single crystal of a lead-free organic-inorganic hybrid perovskite for high-performance photodetector. *Adv. Funct. Mater.* 28:1705467. doi: 10.1002/adfm.201705467
- Jiang, X., Xia, S., Zhang, J., Ju, D., Liu, Y., Hu, X., et al. (2019). Exploring organic metal halides with reversible temperature-responsive dual-emissive photoluminescence. *ChemSusChem* 12, 5228–5232. doi: 10.1002/cssc.201902481
- Ju, D., Dang, Y., Zhu, Z., Liu, H., Chueh, C.-C., Li, X., et al. (2018a). Tunable band gap and long carrier recombination lifetime of stable mixed CH₃NH₃Pb_xSn_{1-x}Br₃ single crystals. *Chem. Mater.* 30, 1556–1565. doi: 10.1021/acs.chemmater.7b04565
- Ju, D., Jiang, X., Xiao, H., Chen, X., Hu, X., and Tao, X. (2018b). Narrow band gap and high mobility of lead-free perovskite single crystal Sn-doped MA3Sb2I9. *J. Mater. Chem. A* 6, 20753–20759. doi: 10.1039/C8TA08315K
- Jun, T., Sim, K., Iimura, S., Sasase, M., Kamioka, H., Kim, J., et al. (2018). Lead-free highly efficient blue-emitting Cs₃Cu₂I₅ with 0D electronic structure. *Adv. Mater.* 30:1804547. doi: 10.1002/adma.201804547
- Kojima, A., Teshima, K., Shirai, Y., and Miyasaka, T. (2009). Organometal halide perovskites as visible-light sensitizers for photovoltaic cells. *J. Am. Chem. Soc.* 131, 6050–6051. doi: 10.1021/ja809598r
- Li, X., Li, B., Chang, J., Ding, B., Zheng, S., Wu, Y., et al. (2018). (C₆H₅CH₂NH₃)₂CuBr₄: a lead-free, highly stable two-dimensional perovskite for solar cell applications. *ACS Appl. Energy Mater.* 1, 2709–2716. doi: 10.1021/acsaem.8b00372
- Lin, K., Xing, J., Quan, L. N., de Arquer, F. P. G., Gong, X., Lu, J., et al. (2018). Perovskite light-emitting diodes with external quantum efficiency exceeding 20 percent. *Nature* 562, 245–248. doi: 10.1038/s41586-018-0575-3
- Ling, Y., Yuan, Z., Tian, Y., Wang, X., Wang, J. C., Xin, Y., et al. (2016). Bright light-emitting diodes based on organometal halide perovskite nanoplatelets. *Adv. Mater.* 28, 305–311. doi: 10.1002/adma.201503954
- Liu, Y., Yang, Z., Cui, D., Ren, X., Sun, J., Liu, X., et al. (2015). Two-Inch-Sized Perovskite CH₃NH₃PbX₃ (X = Cl, Br, I) crystals: growth and characterization. *Adv. Mater.* 27, 5176–5183. doi: 10.1002/adma.201502597
- Liu, Y., Zhang, Y., Zhao, K., Yang, Z., Feng, J., Zhang, X., et al. (2018). A 1300 mm² ultrahigh-performance digital imaging assembly using high-quality perovskite single crystals. *Adv. Mater.* 30:e1707314. doi: 10.1002/adma.201707314
- Lv, X.-H., Liao, W.-Q., Li, P.-F., Wang, Z.-X., Mao, C.-Y., and Zhang, Y. (2016). Dielectric and photoluminescence properties of a layered perovskite-type organic-inorganic hybrid phase transition compound: NH₃(CH₂)₅NH₃MnCl₄. *J. Mater. Chem. C* 4, 1881–1885. doi: 10.1039/C5TC04114G
- Nakayama, Y., Nishihara, S., Inoue, K., Suzuki, T., and Kurmoo, M. (2017). Coupling of magnetic and elastic domains in the organic-inorganic layered perovskite-like (C₆H₅C₂H₄NH₃)₂Fe(II)Cl₄ crystal. *Angew. Chem. Int. Ed. Engl.* 56, 9367–9370. doi: 10.1002/anie.201703898
- Nazarenko, O., Kotyba, M. R., Yakunin, S., Worle, M., Benin, B. M., Raino, G., et al. (2019). Guanidinium and mixed cesium-guanidinium tin(II) bromides: effects of quantum confinement and out-of-plane octahedral tilting. *Chem. Mater.* 31, 2121–2129. doi: 10.1021/acs.chemmater.9b00038
- Park, G., Oh, I. H., Park, J. M. S., Jung, J., You, C. Y., Kim, J. S., et al. (2018). Solvent-dependent self-assembly of two dimensional layered perovskite (C₆H₅CH₂CH₂NH₃)₂MCl₄ (M = Cu, Mn) thin films in ambient humidity. *Sci. Rep.* 8:4661. doi: 10.1038/s41598-018-23012-2
- Rodríguez-Lazcano, Y., Nataf, L., and Rodríguez, F. (2009). Pressure-induced transformation from isolated MnX₄(Td) to exchange-coupled MnX₆(Oh) in A₂MnX₄ (X: Cl, Br) crystals. Structural correlations by time-resolved spectroscopy. *J. Lumin.* 129, 2000–2003. doi: 10.1016/j.jlumin.2009.04.077
- Shrestha, S., Fischer, R., Matt, G. J., Feldner, P., Michel, T., Osvet, A., et al. (2017). High-performance direct conversion X-ray detectors based on sintered hybrid lead triiodide perovskite wafers. *Nat. Photonics.* 11, 436–440. doi: 10.1038/nphoton.2017.94
- Sun, M. E., Li, Y., Dong, X. Y., and Zang, S. Q. (2019). Thermoinduced structural transformation and thermochromic luminescence in organic manganese chloride crystals. *Chem. Sci.* 10, 3836–3839. doi: 10.1039/C8SC04711A
- Sun, X. F., Li, P. F., Liao, W. Q., Wang, Z., Gao, J., Ye, H. Y., et al. (2017). Notable broad dielectric relaxation and highly efficient red photoluminescence in a perovskite-type compound: (N-Methylpyrrolidinium)MnCl₃. *Inorg. Chem.* 56, 12193–12198. doi: 10.1021/acs.inorgchem.7b01553
- Sun, Z., Zeb, A., Liu, S., Ji, C., Khan, T., Li, L., et al. (2016). Exploring a lead-free semiconducting hybrid ferroelectric with a zero-dimensional perovskite-like structure. *Angew. Chem. Int. Ed. Engl.* 55, 11854–11858. doi: 10.1002/anie.201606079
- Tao, K., Li, Y., Ji, C., Liu, X., Wu, Z., Han, S., et al. (2019). A lead-free hybrid iodide with quantitative response to X-ray radiation. *Chem. Mater.* 31, 5927–5932. doi: 10.1021/acs.chemmater.9b02263
- Thirumal, K., Chong, W. K., Xie, W., Ganguly, R., Muduli, S. K., Sherburne, M., et al. (2017). Morphology-independent stable white-light emission from self-assembled two-dimensional perovskites driven by strong exciton-phonon coupling to the organic framework. *Chem. Mater.* 29, 3947–3953. doi: 10.1021/acs.chemmater.7b00073
- Wrighton, M., and Ginley, D. (1974). Excited state decay of tetrahalomanganese(II) complexes. *Chem. Phys.* 4, 295–299. doi: 10.1016/0301-0104(74)80097-2
- Xu, L. J., Sun, C. Z., Xiao, H., Wu, Y., and Chen, Z. N. (2017). Green-light-emitting diodes based on tetrabromide manganese(II) complex through solution process. *Adv. Mater.* 29:1605739. doi: 10.1002/adma.201605739
- Yakunin, S., Protesescu, L., Krieg, F., Bodnarchuk, M. I., Nedelcu, G., Humer, M., et al. (2015). Low-threshold amplified spontaneous emission and lasing from colloidal nanocrystals of caesium lead halide perovskites. *Nat. Commun.* 6:8056. doi: 10.1038/ncomms9056
- Yang, S., Dai, J., Yu, Z., Shao, Y., Zhou, Y., Xiao, X., et al. (2019b). Tailoring passivation molecular structures for extremely small open-circuit voltage loss in perovskite solar cells. *J. Am. Chem. Soc.* 141, 5781–5787. doi: 10.1021/jacs.8b13091
- Yang, S., Xu, Z., Xue, S., Kandlakunta, P., Cao, L., Huang, J. (2019a). Organohalide lead perovskites: more stable than glass under gamma-ray radiation. *Adv. Mater.* 31:e1805547. doi: 10.1002/adma.201805547
- Ye, H. Y., Zhou, Q., Niu, X., Liao, W. Q., Fu, D. W., Zhang, Y., et al. (2015). High-temperature ferroelectricity and photoluminescence in a hybrid organic-inorganic compound: (3-Pyrrolidinium)MnCl₃. *J. Am. Chem. Soc.* 137, 13148–13154. doi: 10.1021/jacs.5b08290
- You, Y. M., Liao, W. Q., Zhao, D., Ye, H. Y., Zhang, Y., Zhou, Q., et al. (2017). An organic-inorganic perovskite ferroelectric with large piezoelectric response. *Science* 357, 306–309. doi: 10.1126/science.aai8535
- Yu, W., Li, F., Yu, L., Niazi, M. R., Zou, Y., Corzo, D., et al. (2018). Single crystal hybrid perovskite field-effect transistors. *Nat. Commun.* 9:5354. doi: 10.1038/s41467-018-07706-9
- Zhang, J., Han, S., Liu, X., Wu, Z., Ji, C., Sun, Z., et al. (2018). A lead-free perovskite-like hybrid with above-room-temperature switching of quadratic nonlinear optical properties. *Chem. Commun.* 54, 5614–5617. doi: 10.1039/C8CC02496K
- Zhang, Y., Liao, W. Q., Fu, D. W., Ye, H. Y., Liu, C. M., Chen, Z. N., et al. (2015). The first organic-inorganic hybrid luminescent multiferroic: (Pyrrolidinium)MnBr₃. *Adv. Mater.* 27, 3942–3946. doi: 10.1002/adma.201501026
- Zhou, L., Liao, J. F., Huang, Z. G., Wei, J. H., Wang, X. D., Chen, H. Y., et al. (2019). Intrinsic self-trapped emission in 0D lead-free (C₄H₁₄

- N2)2 In2 Br10 single crystal. *Angew. Chem. Int. Ed. Engl.* 58, 15435–15440. doi: 10.1002/anie.201907503
- Zhu, H., Fu, Y., Meng, F., Wu, X., Gong, Z., Ding, Q., et al. (2015). Lead halide perovskite nanowire lasers with low lasing thresholds and high quality factors. *Nat Mater.* 14, 636–642. doi: 10.1038/nmat4271
- Zhu, H., Liu, A., Luque, H. L., Sun, H., Ji, D., and Noh, Y. Y. (2019). Perovskite and conjugated polymer wrapped semiconducting carbon nanotube hybrid films for high-performance transistors and phototransistors. *ACS Nano.* 13, 3971–3981. doi: 10.1021/acsnano.8b07567
- Zhumekenov, A. A., Burlakov, V. M., Saidaminov, M. I., Alofi, A., Haque, M. A., Turedi, B., et al. (2017). The role of surface tension in the crystallization of metal halide perovskites. *ACS Energy Lett.* 2, 1782–1788. doi: 10.1021/acsenerylett.7b00468

Conflict of Interest: The authors declare that the research was conducted in the absence of any commercial or financial relationships that could be construed as a potential conflict of interest.

The reviewer JD declared a past co-authorship with the authors XJ, ZC, and XT to the handling editor.

Copyright © 2020 Jiang, Chen and Tao. This is an open-access article distributed under the terms of the Creative Commons Attribution License (CC BY). The use, distribution or reproduction in other forums is permitted, provided the original author(s) and the copyright owner(s) are credited and that the original publication in this journal is cited, in accordance with accepted academic practice. No use, distribution or reproduction is permitted which does not comply with these terms.